Characterizing Nitrogen Sites in Nitrogen-Doped Reduced Graphene Oxide: A Combined Solid-State ^{15}N NMR, XPS and DFT Approach

*Gunwoo Kim,[a,b,e+] Jeongjae Lee,[a,c+] Tao Liu,[a,d] and Clare P. Grey[a,]**

[a]Department of Chemistry, University of Cambridge, Lensfield Road, Cambridge, UK CB2 1EW

[b]Cambridge Graphene Centre, University of Cambridge, Cambridge, UK CB3 0FA

[c]Current Address: School of Earth&Environmental Sciences, Seoul National University, Seoul Korea 08826

[d]Current Address: Shanghai Key Laboratory of Chemical Assessment and Sustainability, Department of Chemistry, Tongji University, Shanghai, China

[e]Current Address: Analytical Sciences Center, LG Energy Solution, Daejeon Korea

+ G. K. and J. L contributed equally to this work.

Corresponding Author

cpg27@cam.ac.uk

Abstract: Despite the potential applications in energy storage and conversion systems such as Li-oxygen batteries and fuel cells, the nature and distribution of doped nitrogen sites in reduced graphene oxides are still not well understood. In this work, we report a combined approach of ^{15}N solid-state nuclear magnetic resonance (NMR) spectroscopy alongside the predominantly used X-ray photoelectron spectroscopy (XPS) to characterize the nitrogen environments in reduced graphene oxides. Application of ^{1}H-^{15}N low-power double quantum cross polarization under fast magic angle spinning with Carr-Purcell-Meiboom-Gill scheme shows selective detection of protonated sites with low-power radiofrequency irradiation. NMR shift calculations of a series of N-containing molecules and a graphene nanoflake model were performed to help interpret the experimental data. This work demonstrates a powerful approach to identify and quantify the different nitrogen environments in doped graphene materials and can also be widely applied to similar graphitic carbon-based materials with other dopants.

TOC GRAPHICS

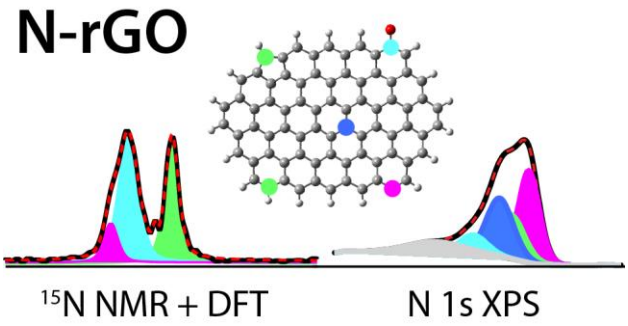

KEYWORDS Doped graphenes, NMR, XPS, *ab initio*, cross polarization

Research on graphene-based materials possessing two-dimensional (2D) carbon structures has gained significant attention due to the versatile functionalities of these materials, originating from the flexibility of tuning pore size/distribution, surface area, and especially, modifying electronic structure in the basal plane by substitution of carbon by other heteroatoms such as boron, nitrogen, sulfur, phosphorus, and halogens.[1–3] There are strong demands for non-metallic catalysts for reactions of significant importance in energy storage and conversion such as hydrogen evolution reaction in water splitting, oxygen reduction reaction in fuel cells and metal-oxygen batteries, and oxygen evolution reactions in metal-oxygen batteries and water splitting.[2,4–7] Current industrial applications heavily rely on the use of metal-based catalysts but many suffer from known drawbacks such as cost, toxicity, and loss of catalytic activity due to poisoning.[2] To tackle the aforementioned problems, the use of various doped-graphene/carbon-based materials has been evaluated in energy-related applications; for example, recent studies demonstrated that introducing heteroatom-dopants such as nitrogen in graphene facilitates oxygen reduction reaction (ORR) in fuel cells operated in aqueous alkaline media.[8,9] Similarly, reduced graphene oxide (rGO) with nitrogen dopants is a promising electrode material with potential use in Li-air batteries,[10–12] these batteries possessing a higher theoretical specific energy density than the conventional Li-ion batteries.[13,14] As nitrogen-containing functional groups are expected to play an important role in the ORR process,[15] fully characterizing the nature of those nitrogen sites is essential to further improvement of oxygen electrocatalysis.

Many previous studies reported N-doped graphenes synthesized by the reaction of graphene oxide, which is prepared by a modified Hummer's method, with several sources of nitrogen such as urea, ammonia, melamine or hydrazine.[3,16,17] The doping level of nitrogen varies from 1-16 atomic % based on the synthetic method, precursors and reaction temperatures.[3,18] Due to the low concentration of dopant nitrogen and lack of crystallinity, previous characterizations of rGOs, especially their nitrogen sites, reported in the literature have been predominantly relied on X-ray Photoelectron Spectroscopy (XPS).[19,20] Four nitrogen environments are commonly reported;

pyridinic (398.1-399.3 eV), pyrrolic (399.8-401.2 eV), graphitic (401.1-402.7 eV), and N-oxide (pyridinic N at ~402.8 eV).[3,17,21] Recent studies have suggested that among these N sites, the major catalytic activity likely stems from pyridinic N sites rather than from all of the others.[22] Full characterization of the functional groups present in N-doped rGO is difficult due to the challenges associated with XPS fitting, often showing the lack of sufficient resolution and peak overlap.[17,21] Thus, other quantitative spectroscopic methods are required to complement the XPS.

Solid-state NMR, being a local characterization technique, offers a promising route to identify and potentially quantify the functional groups. In particular, ^{15}N NMR is particularly promising since ^{15}N is a spin-1/2 nucleus with a wide chemical shift range. However, its measurement suffers from its low natural abundance (0.4 vs. 99.6 % for ^{15}N and ^{14}N, respectively). Solid-state ^{15}N NMR spectroscopy has been employed to characterize the nitrogen environments in graphitic carbon-based materials, revealing useful chemical shift information on diverse nitrogen sites; ^{1}H-^{15}N cross polarization (CP) and ^{15}N direct polarization (DP) magic angle spinning (MAS) NMR measurements of nitrogen–containing carbonaceous solids reported shifts for pyrrolic, graphitic, and pyridinic nitrogen at around -245, -180, and -80 ppm (with respect to CH_3NO_2 (*l*)), respectively.[23] Similarly, more recent ^{15}N MAS NMR measurements of a N-containing pyrolized carbon material identified a combination of pyridinic, graphitic, and edge nitrogen features with the aid of a CP pulse sequence; however poor resolution was observed due to the relatively slow sample spinning (MAS rate = 20 kHz) and moderate field (11.7 T).[24] In a different study, two distinct graphitic N shifts of -180 (N bonded to three carbons) and -223 ppm (N bonded to two carbons) in a melem unit have been reported alongside *ab initio* calculations of ^{15}N and ^{13}C-enriched graphitic carbon nitride (g-C_3N_4).[25] Another NMR study of hydrazine-treated graphite oxide reported that pyrazole formation at edges gives rise to a broad ^{15}N resonance at -200 ppm.[16]

In all these measurements, relatively slow (10-20 kHz) sample spinning was employed to ensure reasonable sensitivity of dilute ^{15}N nuclei by sufficient sampling amount. To enhance the site resolution, fast spinning (>40 kHz) would be desirable; the normal disadvantages of such fast MAS, however, are: (a) smaller available rotor sample volume and poorer signal sensitivity, and (b) an increase in the CP radiofrequency (rf) power to satisfy the Hartmann-Hahn (HH) condition, which is likely to result in sample degradation due to stronger rf heating in these conductive graphenes.[26] To overcome (a), we have employed ^{15}N enrichment of the dopant precursor, together with Carr-Purcell-Meiboom-Gill (CPMG) detection of multiple echoes to drastically improve the sensitivity;[27] (b) was solved by employing a low-power *Double Quantum* (DQ) HH condition in the CP sequence.[28] In brief, this modifies the normal *Zero Quantum* HH condition of $\omega_H = \omega_C \pm n\omega_r$ (where ω_H, ω_C, ω_r are the proton rf, carbon rf, and MAS frequencies, respectively) to $\omega_H + \omega_C = n\omega_r$, thereby allowing polarization transfer under low-power irradiation and consequently less sample heating. As we will show, a combination of DP-CPMG and DQ-CP-CPMG sequences under fast MAS yields high resolution ^{15}N spectra in N-rGO in moderate measurement time with site-specific observation, which would not otherwise be possible with simple echoes under slow MAS.

Ab initio calculations of NMR shifts are almost routinely performed for molecular systems,[29] but only a few systematic studies on the ^{15}N isotope are reported in the literature.[30–33] Care should also be taken when comparing chemical shifts as ^{15}N shifts are often referenced to different compounds (NH_3 (*l*), CH_3NO_2 (*l*), NH_4Cl (*s*), or NH_4NO_3 (*s*)).[34] Furthermore, as nitrogen in N-rGO is in a heterocyclic sp^2 environment, a different shielding-shift relationship to other sp^3-nitrogen environments may be expected. Hence, we have performed a systematic *ab initio* study of ^{15}N shifts in aromatic N-heterocycles to aid our interpretation of the N-rGO NMR spectra.

Hence, in this work, we prepared a ^{15}N-enriched N-rGO, and used a variety of solid-state ^{15}N NMR experiments aided with: (i) fast spinning for enhanced resolution; (ii) CPMG pulse sequence for NMR signal enhancement;[27] and (iii) $^1H \rightarrow {}^{15}N$ low-power DQ CP pulse sequence under fast MAS for enhanced signal and site-specific observation.[28] The NMR results are in good agreement with the XPS characterization. *Ab initio* calculations have been employed to characterize the NMR shifts of nitrogen functional groups in the graphene: graphene nanoflake model structures were constructed to help assign the experimental ^{15}N NMR spectrum, providing a good agreement with the previous experimental and computational studies. Our work provides insights into the structure of nitrogen sites on graphene and the approach is widely applicable for studying similar graphitic carbon-based materials.

The N-rGO was synthesized by a two-step process reported previously[21] involving hydrothermal reaction of a mixture of urea and graphite oxide (GO), dispersed in aqueous solution and the subsequent thermal reduction of the resulting solid mixture at 600 ºC in an argon flow. The structural integrity of the prepared N-rGO was characterized by powder X-ray diffraction (PXRD), Raman, scanning electron microscopy (SEM), and transmission electron microscopy (TEM). Figure 1a shows the XRD patterns of GO, N-rGO, and pristine graphite for comparison. The (002) reflection of GO and N-rGO corresponds to the broad reflections at 10.0 and 26.4º 2θ respectively. The peak shift of the (002) reflection from 10º for GO to 26.4º, 2θ for N-rGO indicates a significant decrease in the interlayer spacing from 8.84 Å to 3.37 Å. As previously reported, this change is due to removal of various oxygen functional groups (hydroxyl, epoxy, carbonyl, *etc.*) upon thermal reduction.[35] The broadening of the (002) reflection in graphite-like materials is commonly associated with the turbostratic nature, fluctuation in interlayer spacing, and/or variation in the local curvature of the graphene layers.[36] Raman spectra of both rGO and N-rGO (Figure 1b) show two dominant and characteristic peaks known as D and G bands at ~1330 and ~1590 cm^{-1}, respectively. Unlike graphenes, the Raman spectrum of the pristine graphite reference displays a very narrow and intense G band along with very weak D and noticeably intense 2D bands. The G band originates from the Raman-active in-plane E_{2g} mode. The D band stems from the in-plane breathing modes (A_{1g}) of six-atom rings, which are only Raman-active in the presence of defects in the rings.[37] Therefore, the intensity ratio of the D and G bands (I_D/I_G) is also a sensitive measure of disorder in graphitic structures. The slightly increased I_D/I_G ratio of 1.3 is obtained from N-rGO with respect to 1.2 from rGO (see also Figure S1), the increase being tentatively ascribed to the defects induced by nitrogen dopants in the N-rGO. The graphitic morphologies of doped rGO also have been confirmed by SEM and TEM. SEM images of pristine and doped rGO (Figure 1c and

S2 in SI) show very similar, hierarchical macroporous and uniform structures. No segregation is observed from addition of urea (for doping), which was mostly removed by the thermal reduction process. A TEM image of doped rGO in Figure 1d exhibits lattice fringes of graphene layers.

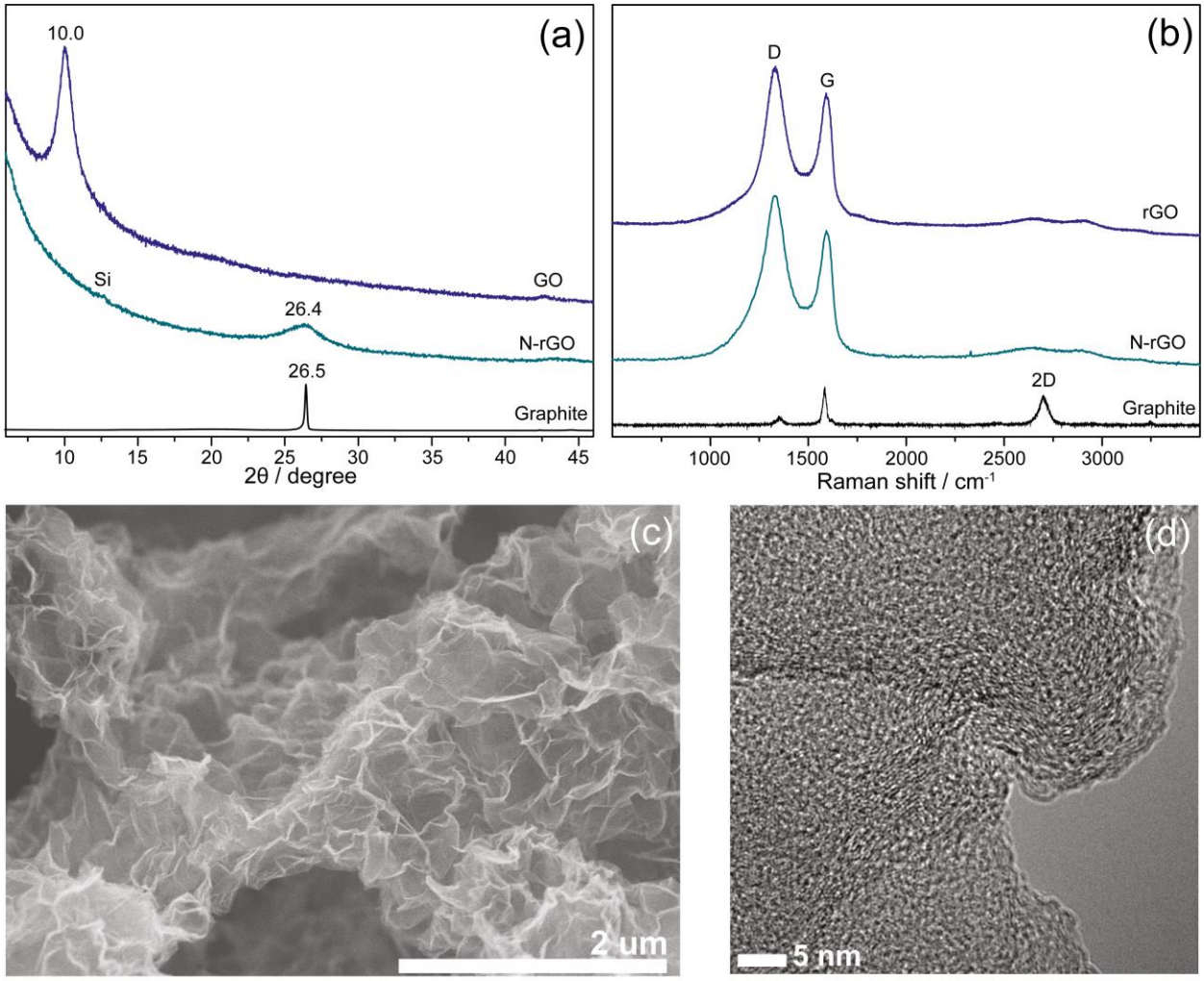

Figure 1. (a) XRD patterns of N-rGO and GO, (b) Raman spectra of N-rGO and rGO, and (c-d) SEM and TEM images of N-rGO, respectively. In both the XRD and Raman data, measurements of pristine graphite are also shown for comparison.

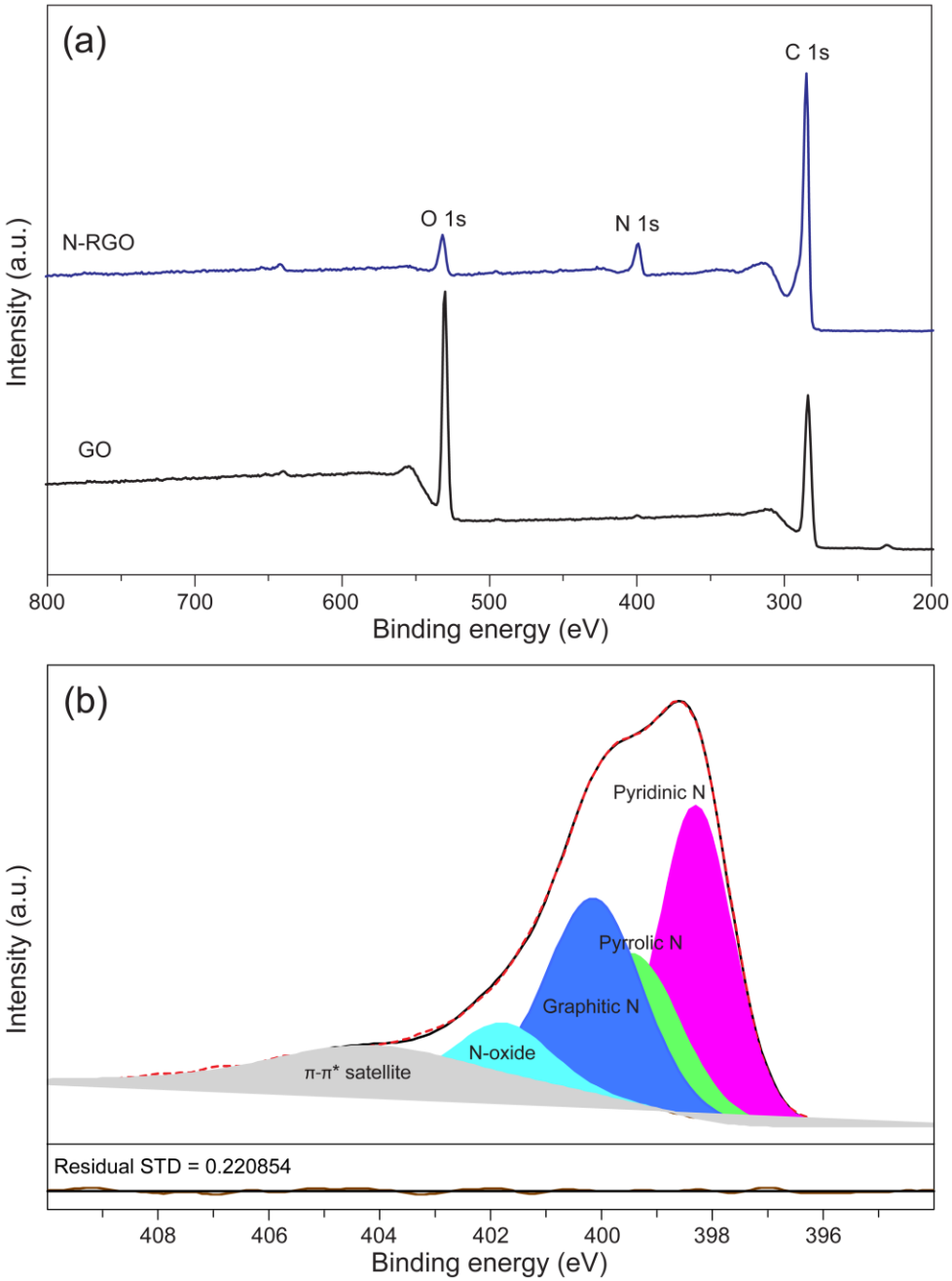

Figure 2. (a) XPS survey spectrum of N-rGO and GO, and (b) high resolution N 1s XPS spectrum (black solid line). The experimental and a total fit are shown as black solid and red dashed lines; the peak areas are filled with various colors denoting individual fits to different N species.

XPS has been employed to confirm the extent of nitrogen doping into the graphitic structure and to assign various nitrogen sites. XPS survey spectra of N-rGO and GO are shown in Figure 2a. The N-rGO survey exhibts a major C 1s peak with two minor O 1s and N 1s peaks, indicating the nitrogen dopant implanted in the structure; a doping level of ~7 atomic % nitrogen is estimated. A high resolution N 1s XPS spectrum (Figure 2b) shows two overlapped peaks with a broad tail at a higher binding energy region and its spectral deconvolution further reveals at least four nitrogen environments corresponding to pyridinic (398.3 eV with 33.6 %), pyrrolic (399.4 eV with 20.4 %), graphitic (400.1 eV with 27.4 %), and N-oxide (401.8 eV with 8.70 %) with $\pi - \pi^*$ satellite at 404.2 eV (9.96%), making use of assignments from previous XPS data of N-doped carbon structures.[18,21] The relative composition of the various species differs however, with higher pyrrolic and pyridinic compositions alongside a lower graphitic nitrogen content being observed due to the lower reduction temperature applied (600 ºC) compared to the temperature used to prepare the previously reported sample.[21]

A solid-state ^{13}C NMR spectrum of pristine rGO and N-rGO are shown in Figure S3. The two spectra are only marginally different, with the N-rGO showing a slightly higher peak intensity around the 150 ppm region (where sp^2 C-N bonded carbons are expected to resonate); but in general the resolution is insufficient to distinguish between different carbon environments. Therefore, a solid-state ^{15}N CPMG MAS NMR measurement of N-rGO has been used to directly observe various nitrogen environments in the graphitic structure. The ^{15}N direct polarization (DP) CPMG spectrum (Figure 3a) contains two overlapping peaks with small shoulders. The lineshape is much broader than the reported ^{15}N spectrum of graphitic carbon nitride (g-C_3N_4), this being ascribed to the distribution of nitrogen dopants and conductive nature of graphene. The ^{15}N spectrum is deconvoluted into four peaks at -70, -116, -183, and -227 ppm, which we assign as pyridinic, N-oxide, graphitic, and pyrrolic/pyridinium nitrogen sites, respectively (*vide infra*).

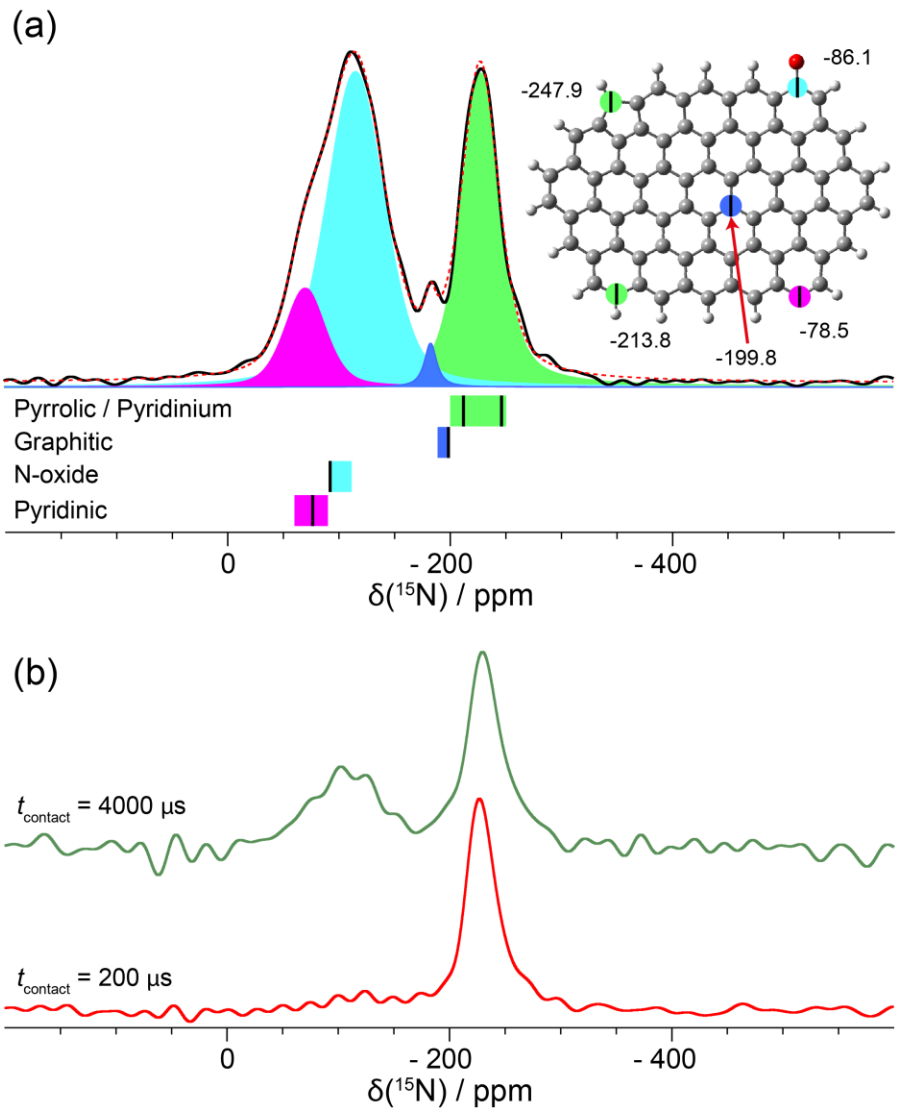

Figure 3. Solid-state (a) ^{15}N DP-CPMG and (b) ^{1}H-^{15}N CP-CPMG MAS NMR spectra of N-rGO, acquired at a 16.4 T with a MAS frequency of 50 kHz. Experimental and total fits are shown as black solid and red dashed lines, respectively; peak areas are filled with different colors to identify and assign the individual peaks. The range of shifts obtained from singly-doped nanoflakes (model A) are shown as colored bars, with black line denoting the shifts obtained from the multiple-doped nanoflake (model B; also shown as an inset on the right hand side). In the model structure, gray, white, and red balls denote carbon, hydrogen, and oxygen atoms, respectively. CP contact times are shown in the figure.

To aid the identification of protonated species through spectral editing, a high resolution ^{1}H-^{15}N CP CPMG NMR measurents under fast MAS (50 kHz) of N-rGO was also performed (Figure 3b). With a short CP contact time of 200 μs, the signal at -227 ppm is selectively excited, indicating that this site is directly bonded to a proton. Thus, this peak must be assigned to either pyrrolic (N-H) or pyridinium (N^{+}-H) environments, consistent with the previous report on N-containing pyrolized carbon.[24] The calculated proton shieldings of pyrrolic and pyridinium species in the nanoflake model (*vide infra*) are similar (20.8 and 21.8 ppm, respectively). With a longer CP contact time of 4000 μs, other N sites more distant from the protons also start to build up in intensity, resembling the DP CPMG spectrum. Of note, the pyridinic and N-oxide overlapping resonance is now seen (-50 to -150 ppm), consistent with the location of these environments on the edge of the graphene flakes, close to the terminating C-H species. The graphitic N environment (-190 ppm) is not observed on this CP spectrum, consistent with its location in the center of the flakes.

Despite the spectral editing with CP technique, the overlapping high-frequency signals are still not resolved clearly. Hence, *ab initio* NMR chemical shift calculations were performed on N-containing model systems to aid the assignment of different nitrogen species. The investigated models include (i) 71 N-containing small heterocyclic molecules and (ii) graphene flakes doped with various nitrogen functional groups. Figure 4 shows the relationship of the ^{15}N chemical shielding (σ_{iso}) in N-heterocycles *versus* their ^{15}N isotropic chemical shifts (δ_{iso}), together with approximate shift ranges for each functional group. A linear relation is found between σ_{iso} and δ_{iso}, with a functional form of $\delta_{iso} = -0.925\sigma_{iso} - 125.05$ relative to liquid nitromethane (CH_3NO_2). The shifts can be grouped into four regions according to the functional groups: (i) diazine N=N (50 to -50 ppm), (ii) pyridinic N, N-oxide, and pyrryl N (-50 to -150 ppm), (iii) graphitic/tertiary N (-150 to -200 ppm), and (iv) pyrrolic N (-200 to -300 ppm). Considering the different shift ranges, it is observed that (i) diazine N=N group is highly deshielded, possibly due to the more electronegative nature of the nitrogen relative to carbon; (ii) pyridinic, pyrryl, and N-oxides share similar ranges of shifts, although N-oxides have narrower, less shielded shift range (-50 to -100 ppm; due to oxygen coordination) compared to the other the two (-50 to -150 ppm); and (iii) graphitic and pyrrolic shifts are well separated from the others, so these should be easily identified in a spectrum.

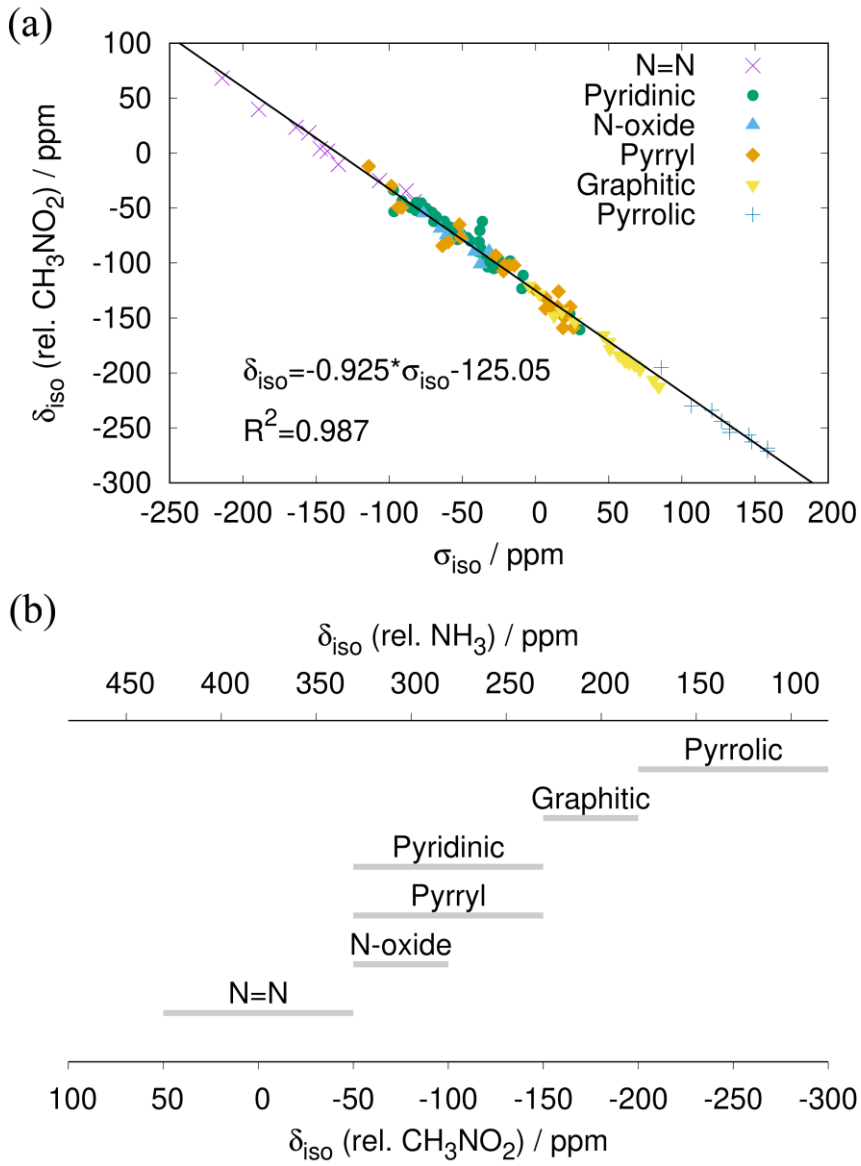

Figure 4. (a) Calculated ^{15}N isotropic chemical shielding (σ_{iso}) *versus* experimental isotropic chemical shift (δ_{iso}) in a series of small N-heterocyclic molecules. The linear regression shows the trend between δ_{iso} and σ_{iso}. (b) Calculated ^{15}N chemical shift ranges for the collection of heterocyclic molecules presented in (a), referenced to NH_3 (*l*) and CH_3NO_2 (*l*).

The calculated range of shifts is in agreement with previous reports by Solum *et al.* on nitrogen heterocycles, where the shifts were referenced by simply subtracting the σ_{iso} from the nitromethane reference, effectively setting a = -1 in the regression as expected from the shielding-shift relationship.[32] However, the value of a = -0.925 clearly deviates from -1, which is generally ascribed to deficiencies in the functionals used in the DFT calculations (the so-called 'self-interaction error');[38] the added degree of freedom by performing a two-variable linear regression (slope and intercept) is expected to yield a more accurate shielding-shift relationship. A more recent study by Xin *et al.* on ^{15}N shifts of general nitrogen functional groups found the relationship $\delta_{iso} = -0.978\sigma_{iso} - 126.77$, which is close to the current result.[33] However, it needs to be stressed that a more extensive cc-pDVZ basis set was used in their study, compared to our 6-31+G(d,p); good agreement between the two regression data shows that a dual basis scheme with cheaper 6-31G(d)/6-31+G(d,p) basis sets could be used to calculate the shielding, which becomes important for evaluating the shielding in the larger graphene nanoflake models used here (*vide infra*).

To simulate more realistic doped nitrogen environments, two classes of N-doped graphite models were then constructed based on an undoped graphene nanoflake, composed of 77 carbon atoms: (i) 22 model structures simulating single-nitrogen doping by five different functional groups (N-oxide, graphitic, pyridine, pyridinium, and pyrrolic), with each nitrogen placed in different positions relative to the flake edge, denoted model A and (ii) one structure of multiple-nitrogen doping (one of each functional group) to simulate a more realistic scenario at 6.5 atomic %, denoted model B. The range of shifts obtained from singly-doped model A are shown below the experimental spectra in Figure 3a, alongside the values of shifts obtained from the multiple-doped graphene flake of model B (shown on inset). The calculated ranges of the shifts correspond well to the experimental spectrum, shown with the same color scheme on both the deconvoluted peaks and the model structure of graphene nanoflake.

These DFT calculations, therefore, further corroborate the assignment of -227 ppm peak to pyrrolic/pyridinium species from the CP spectra; furthermore, the partially overlapping resonances at -70, -116, and -183 ppm are now unambiguously assigned to pyridinic, N-oxide, and graphitic species, respectively. Our assignments are also in good agreement with the previous NMR study by MacIntosh *et al.*, although the resolution and sensitivity of their ^{15}N spectrum is poorer due to the slower MAS rate used (15 kHz *versus* 50 kHz used in this work).[24] We also note that the nature of our sample, a reduced graphene oxide prepared with nitrogen dopants, is significantly different to their work, in which a N-containing carbon was prepared from pyrolyzing a polymerized aniline precursor. The peak at -183 ppm is also in a good agreement with the shift from the reported graphitic carbon nitride[25] and it is assigned to graphitic N. Of note, the intensity of the shift corresponding to graphitic N (a blue peak in Figure 3) is noticeably lower than what expected from the XPS data. This could arise from a very different spin-lattice relaxation behavior of graphitic N (the reported T_1 is >1000 s and thus the signal being saturated by the use of a shorter recycle delay of 5 s).[25] A distribution of graphitic nitrogen resonances over a broad range is not expected, as

evidenced from the narrow range of graphitic ^{15}N shifts in a series of graphite nanoflake models doped with graphitic nitrogen placed at different positions (model A; Figure 3a, blue bar).

Our work demonstrated that various nitrogen sites in nitrogen-doped reduced graphene oxide can be identified and assigned by a combined approach of XPS, NMR, and *ab initio* calculations. Along with ^{15}N enrichment, ^{15}N CPMG and CP pulse sequences have been employed for NMR signal enhancement to determine the nature of doping in reduced graphene oxide. Fast sample spinning, combined with CP under fast MAS conditions, enables high resolution spectra to be acquired to allow clear assignments of various nitrogen sites. At least four nitrogen sites are characterized and a good agreement between our experimental and computational data is obtained. This study establishes a baseline for characterizing various nitrogen environments in graphenes and heterocyclics in general and can also be extended to study similar graphitic carbon-based materials with other dopants.

Acknowledgements

G.K. and C.P.G. thank EUHorizon 2020 GrapheneCore1-No.696656 for research funding. T.L. thanks Darwin College for Schlumberger Fellowship and Innovate UK for research funding. All authors thank Dr. Robert Weatherup and Dr. Chao Xu for fruitful discussions about XPS data analysis, Mr. Chris Amey for XPS measurements, and Dr. Jingyu Lu for TEM measurements. This research used resources of the Center for Functional Nanomaterials, which is a U.S. DOE Office of Science Facility, and the Scientific Data and Computing Center, a component of the Computational Science Initiative, at Brookhaven National Laboratory under Contract No. DE-SC0012704.

Notes

The authors declare no competing financial interests.

Supporting Information

Supporting information including experimental details, Raman and SEM images, and 13C CPMG NMR spectra, and library of calculated ^{15}N chemical shielding versus chemical shifts are available.

References

(1) Eigler, S.; Hirsch, A. Chemistry with Graphene and Graphene Oxide - Challenges for Synthetic Chemists. *Angewandte Chemie - International Edition* **2014**, *53* (30), 7720–7738.

https://doi.org/10.1002/anie.201402780.
(2) Liu, X.; Dai, L. Carbon-Based Metal-Free Catalysts. *Nature Reviews Materials* **2016**, *1*, 1–12. https://doi.org/10.1038/natrevmats.2016.64.
(3) Wang, H.; Maiyalagan, T.; Wang, X. Review on Recent Progress in Nitrogen-Doped Graphene: Synthesis, Characterization, and Its Potential Applications. *ACS Catalysis* **2012**, *2* (5), 781–794. https://doi.org/10.1021/cs200652y.
(4) Shui, J.; Lin, Y.; Connell, J. W.; Xu, J.; Fan, X.; Dai, L. Nitrogen-Doped Holey Graphene for High-Performance Rechargeable Li-O2 Batteries. *ACS Energy Letters* **2016**, *1* (1), 260–265. https://doi.org/10.1021/acsenergylett.6b00128.
(5) Zhu, Y. P.; Guo, C.; Zheng, Y.; Qiao, S.-Z. Surface and Interface Engineering of Noble-Metal-Free Electrocatalysts for Efficient Energy Conversion Processes. *Accounts of Chemical Research* **2017**, *50* (4), 915–923. https://doi.org/10.1021/acs.accounts.6b00635.
(6) Hu, C.; Dai, L. Carbon-Based Metal-Free Catalysts for Electrocatalysis beyond the ORR. *Angewandte Chemie International Edition* **2016**, *55* (39), 11736–11758. https://doi.org/10.1002/anie.201509982.
(7) Georgakilas, V.; Tiwari, J. N.; Kemp, K. C.; Perman, J. A.; Bourlinos, A. B.; Kim, K. S.; Zboril, R. Noncovalent Functionalization of Graphene and Graphene Oxide for Energy Materials, Biosensing, Catalytic, and Biomedical Applications. *Chemical Reviews* **2016**, *116* (9), 5464–5519. https://doi.org/10.1021/acs.chemrev.5b00620.
(8) Gong, K.; Du, F.; Xia, Z.; Durstock, M.; Dai, L. Nitrogen-Doped Carbon Nanotube Arrays with High Electrocatalytic Activity for Oxygen Reduction. *Science* **2009**, *323* (5915), 760–764. https://doi.org/10.1126/science.1168049.
(9) Shui, J.; Wang, M.; Du, F.; Dai, L. N-Doped Carbon Nanomaterials Are Durable Catalysts for Oxygen Reduction Reaction in Acidic Fuel Cells. *Science Advances* **2015**, *1* (1), e1400129–e1400129. https://doi.org/10.1126/sciadv.1400129.
(10) Wang, M.; Yao, Y.; Tang, Z.; Zhao, T.; Wu, F.; Yang, Y.; Huang, Q. Self-Nitrogen-Doped Carbon from Plant Waste as an Oxygen Electrode Material with Exceptional Capacity and Cycling Stability for Lithium–Oxygen Batteries. *ACS Applied Materials & Interfaces* **2018**, *10* (38), 32212–32219. https://doi.org/10.1021/acsami.8b11282.
(11) Shui, J.; Lin, Y.; Connell, J. W.; Xu, J.; Fan, X.; Dai, L. Nitrogen-Doped Holey Graphene for High-Performance Rechargeable Li–O $_2$ Batteries. *ACS Energy Letters* **2016**, *1* (1), 260–265. https://doi.org/10.1021/acsenergylett.6b00128.
(12) Shu, C.; Li, B.; Zhang, B.; Su, D. Hierarchical Nitrogen-Doped Graphene/Carbon Nanotube Composite Cathode for Lithium-Oxygen Batteries. *ChemSusChem* **2015**, *8* (23), 3973–3976. https://doi.org/10.1002/cssc.201501169.
(13) Bruce, P. G.; Freunberger, S. A.; Hardwick, L. J.; Tarascon, J.-M. Li–O2 and Li–S Batteries with High Energy Storage. *Nature Materials* **2011**, *11* (02), 172–172. https://doi.org/10.1038/nmat3237.
(14) Lu, Y.; Gallant, B. M.; Kwabi, D. G.; Harding, J. R.; Mitchell, R. R.; Whittingham, M. S.; Shao-Horn, Y. Lithium–Oxygen Batteries: Bridging Mechanistic Understanding and Battery Performance. *Energy & Environmental Science* **2013**, *6* (3), 750. https://doi.org/10.1039/c3ee23966g.
(15) Chen, P.; Xiao, T. Y.; Qian, Y. H.; Li, S. S.; Yu, S. H. A Nitrogen-Doped Graphene/Carbon Nanotube Nanocomposite with Synergistically Enhanced Electrochemical Activity. *Advanced Materials* **2013**, *25* (23), 3192–3196. https://doi.org/10.1002/adma.201300515.
(16) Park, S.; Hu, Y.; Hwang, J. O.; Lee, E.-S.; Casabianca, L. B.; Cai, W.; Potts, J. R.; Ha, H.-

W.; Chen, S.; Oh, J.; Kim, S. O.; Kim, Y.-H.; Ishii, Y.; Ruoff, R. S. Chemical Structures of Hydrazine-Treated Graphene Oxide and Generation of Aromatic Nitrogen Doping. *Nature Communications* **2012**, *3* (638), 1–8. https://doi.org/10.1038/ncomms1643.

(17) Long, D.; Li, W.; Ling, L.; Miyawaki, J.; Mochida, I.; Yoon, S. H. Preparation of Nitrogen-Doped Graphene Sheets by a Combined Chemical and Hydrothermal Reduction of Graphene Oxide. *Langmuir* **2010**, *26* (20), 16096–16102. https://doi.org/10.1021/la102425a.

(18) Kuroki, S.; Nabae, Y.; Chokai, M.; Kakimoto, M. A.; Miyata, S. Oxygen Reduction Activity of Pyrolyzed Polypyrroles Studied By15N Solid-State NMR and XPS with Principal Component Analysis. *Carbon* **2012**, *50* (1), 153–162. https://doi.org/10.1016/j.carbon.2011.08.014.

(19) Wang, X.; Li, X.; Zhang, L.; Yoon, Y.; Weber, P. K.; Wang, H.; Guo, J.; Dai, H. N-Doping of Graphene Through Electrothermal Reactions with Ammonia. *Science* **2009**, *324* (5928), 768–771.

(20) Li, X.; Wang, H.; Robinson, J. T.; Sanchez, H.; Diankov, G.; Dai, H. Simultaneous Nitrogen Doping and Reduction of Graphene Oxide. *Journal of the American Chemical Society* **2009**, *131* (43), 15939–15944. https://doi.org/10.1021/ja907098f.

(21) Panomsuwan, G.; Saito, N.; Ishizaki, T. Nitrogen-Doped Carbon Nanoparticle–Carbon Nanofiber Composite as an Efficient Metal-Free Cathode Catalyst for Oxygen Reduction Reaction. *ACS Applied Materials & Interfaces* **2016**, *8* (11), 6962–6971. https://doi.org/10.1021/acsami.5b10493.

(22) Guo, D.; Shibuya, R.; Akiba, C.; Saji, S.; Kondo, T.; Nakamura, J. Active Sites of Nitrogen-Doped Carbon Materials for Oxygen Reduction Reaction Clarified Using Model Catalysts. *Science* **2016**, *351* (6271), 361–365. https://doi.org/10.1126/science.aad0832.

(23) Kelemen, S. R.; Afeworki, M.; Gorbaty, M. L.; Kwiatek, P. J.; Solum, M. S.; Hu, J. Z.; Pugmire, R. J. XPS and 15N NMR Study of Nitrogen Forms in Carbonaceous Solids. *Energy and Fuels* **2002**, *16* (6), 1507–1515. https://doi.org/10.1021/ef0200828.

(24) MacIntosh, A. R.; Jiang, G.; Zamani, P.; Song, Z.; Riese, A.; Harris, K. J.; Fu, X.; Chen, Z.; Sun, X.; Goward, G. R. Phosphorus and Nitrogen Centers in Doped Graphene and Carbon Nanotubes Analyzed through Solid-State NMR. *Journal of Physical Chemistry C* **2018**, *122* (12), 6593–6601. https://doi.org/10.1021/acs.jpcc.7b11671.

(25) Hu, Y.; Shim, Y.; Oh, J.; Park, S.; Park, S.; Ishii, Y. Synthesis of 13 C-, 15 N-Labeled Graphitic Carbon Nitrides and NMR-Based Evidence of Hydrogen-Bonding Assisted Two-Dimensional Assembly. *Chemistry of Materials* **2017**, *29* (12), 5080–5089. https://doi.org/10.1021/acs.chemmater.7b00069.

(26) Haw, J. F.; Campbell, G. C.; Crosby, R. C. Experimental Considerations in Variable-Temperature Solid-State Nuclear Magnetic Resonance with Cross Polarization and Magic-Angle Spinning. *Analytical Chemistry* **1986**, *58* (14), 3172–3177. https://doi.org/10.1021/ac00127a056.

(27) Meiboom, S.; Gill, D. Modified Spin-Echo Method for Measuring Nuclear Relaxation Times. *Review of Scientific Instruments* **1958**, *29* (8), 688–691. https://doi.org/10.1063/1.1716296.

(28) Laage, S.; Sachleben, J. R.; Steuernagel, S.; Pierattelli, R.; Pintacuda, G.; Emsley, L. Fast Acquisition of Multi-Dimensional Spectra in Solid-State NMR Enabled by Ultra-Fast MAS. *Journal of Magnetic Resonance* **2009**, *196* (2), 133–141. https://doi.org/10.1016/j.jmr.2008.10.019.

(29) Lodewyk, M. W.; Siebert, M. R.; Tantillo, D. J. Computational Prediction of 1H and 13C

Chemical Shifts: A Useful Tool for Natural Product, Mechanistic, and Synthetic Organic Chemistry. *Chemical Reviews* **2012**, *112* (3), 1839–1862. https://doi.org/10.1021/cr200106v.
(30) Olsson, L.; Cremer, D. Prediction of Nitrogen and Oxygen NMR Chemical Shifts in Organic Compounds by Density Functional Theory. *The Journal of Physical Chemistry* **1996**, *100* (42), 16881–16891. https://doi.org/10.1021/jp961316p.
(31) Marek, R.; Brus, J.; Toušek, J.; Kovács, L.; Hocková, D. N7- and N9-Substituted Purine Derivatives: A 15N NMR Study. *Magnetic Resonance in Chemistry* **2002**, *40* (5), 353–360. https://doi.org/10.1002/mrc.1020.
(32) Solum, M. S.; Altmann, K. L.; Strohmeier, M.; Berges, D. A.; Zhang, Y.; Facelli, J. C.; Pugmire, R. J.; Grant, D. M. 15N Chemical Shift Principal Values in Nitrogen Heterocycles. *Journal of the American Chemical Society* **1997**, *119* (41), 9804–9809. https://doi.org/10.1021/ja964135+.
(33) Xin, D.; Sader, C. A.; Fischer, U.; Wagner, K.; Jones, P.-J.; Xing, M.; Fandrick, K. R.; Gonnella, N. C. Systematic Investigation of DFT-GIAO 15N NMR Chemical Shift Prediction Using B3LYP/Cc-PVDZ: Application to Studies of Regioisomers{,} Tautomers{,} Protonation States and N-Oxides. *Org. Biomol. Chem.* **2017**, *15* (4), 928–936. https://doi.org/10.1039/C6OB02450E.
(34) Bertani, P.; Raya, J.; Bechinger, B. 15N Chemical Shift Referencing in Solid State NMR. *Solid State Nuclear Magnetic Resonance* **2014**, *61–62*, 15–18. https://doi.org/10.1016/j.ssnmr.2014.03.003.
(35) Jeong, H.-K.; Lee, Y. P.; Lahaye, R. J. W. E.; Park, M.-H.; An, K. H.; Kim, I. J.; Yang, C.-W.; Park, C. Y.; Ruoff, R. S.; Lee, Y. H. Evidence of Graphitic AB Stacking Order of Graphite Oxides. *Journal of the American Chemical Society* **2008**, *130* (4), 1362–1366. https://doi.org/10.1021/ja076473o.
(36) Li, Z. Q.; Lu, C. J.; Xia, Z. P.; Zhou, Y.; Luo, Z. X-Ray Diffraction Patterns of Graphite and Turbostratic Carbon. *Carbon* **2007**, *45* (8), 1686–1695. https://doi.org/10.1016/j.carbon.2007.03.038.
(37) Ferrari, A. C.; Basko, D. M. Raman Spectroscopy as a Versatile Tool for Studying the Properties of Graphene. *Nature Nanotechnology* **2013**, *8* (4), 235–246. https://doi.org/10.1038/nnano.2013.46.
(38) Laskowski, R.; Blaha, P.; Tran, F. Assessment of DFT Functionals with NMR Chemical Shifts. *Physical Review B* **2013**, *87* (19). https://doi.org/10.1103/PhysRevB.87.195130.